AUTOMATIC PROCEDURE FOR THERMAL NDE OF DELAMINATIONS IN CFRP BY USING NEURAL NETWORKS

S. Marinetti, P.G. Bison, E. Grinzato
Istituto per la Tecnica del Freddo
Consiglio Nazionale delle Ricerche
35127-Padova (Italy)

G. Manduchi
Istituto Gas Ionizzati
Consiglio Nazionale delle Ricerche
35127-Padova (Italy)

INTRODUCTION

This work is a first step in detecting and characterizing defects in an automatic way by using artificial intelligence. Transient thermal NDE by IR thermography is the method used for such a purpose. Data are processed by Neural Networks.

Objectives: 1) avoiding participation of an expert operator in selecting a reference zone (non-defect area); 2) improvement in dealing with the problem of uneven heating (both the different absorptivity and the non uniformity of the heating source); 3) taking into account the case of a strong 2D diffusion, as it is for CFRP where the thermal diffusivity along the carbon fiber texture (generally parallel to the surface of the object) assumes values two times greater than the in depth diffusivity.

EXPERIMENTAL SET UP

Equipment

The experimental set up, shown in Figure 1, consists of a heating system, an acquisition system and a trigger box synchronizing all the devices. The heating system consists of two banks with 8 IR lamps each one with a total power of 32 kW. The acquisition system is the Thermovision™-900 imager from AGEMA Inc. (Sweden) that may record images or sequences of images in the IR LW band (8-14 μm) in digital format 272 x 136 pixels with resolution of 12 bit/pixel. The experiments on the CFRP specimen were carried out using a heating time of 5 s and acquiring a sequence of 80 images with a sampling time of 1 s.

Specimen characteristics

The CFRP specimen was prepared and provided by the Italian Air Force. It contains a set of 9 defects whose occurrence could be considered very likely in real cases. The specimen, composed of 20 plies of carbon fibers, measures 300 x 300 x 5 mm. The defects are organized in row and columns as it is shown in Figure 2. They were made inserting pieces of Teflon™ between two successive plies.

Review of Progress in Quantitative Nondestructive Evaluation, Vol. 16
Edited by D.O. Thompson and D E. Chimenti, Plenum Press, New York, 1997

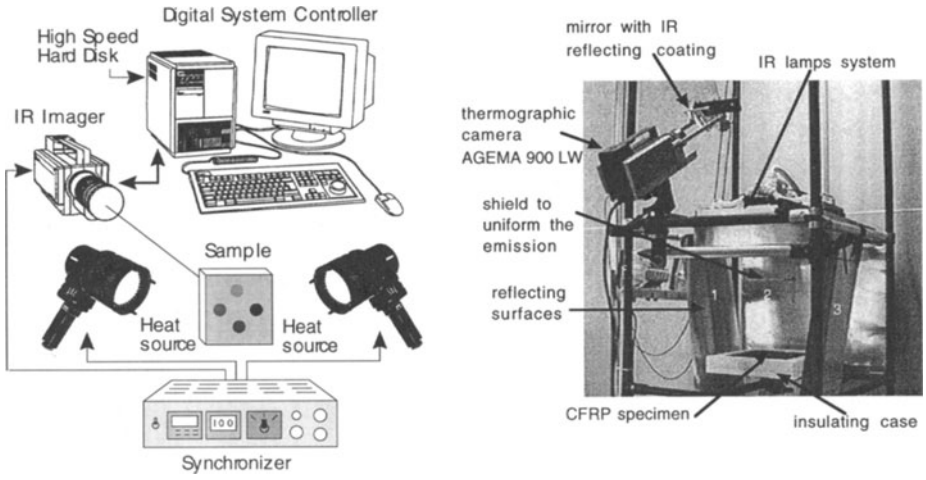

Figure 1. Experimental set up.

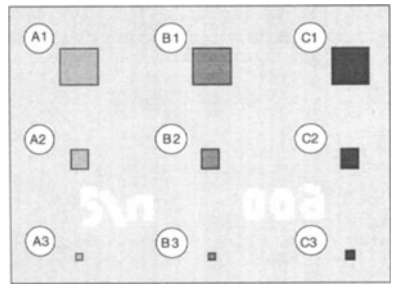

Figure 2. Scheme of CFRP specimen.

In the first column three defects with dimensions 12 x 12, 6 x 6 and 4 x 4 mm were inserted under the first ply (at a depth of 0.25 mm). Other 3 defects with the same dimensions were located under the 5th ply (at a depth of 1.25 mm) and the last 3 defects under the 10th ply (at a depth of 2.5 mm). See Table I.

It is worth noticing that the specimen presents an area with different absorptivity due to a writing on the surface. During the heating, such a zone absorbs a different amount of energy and its temperature differs from the surroundings. Since a defect could behave at the same way, a variation of absorptivity represents a source of false alarms.

THERMAL TOMOGRAPHY

Thermal tomography [1] consists in the characterization of defects inside opaque materials, recovering the internal structure of the body layer by layer. Thermal tomography algorithm works on sequences of IR images grabbed during the thermal evolution of a heated surface. It implies the following steps:

- space domain analysis to locate a sound area as reference;
- time domain analysis to compare the temperature evolution of any point or area with the reference one.

Several informative parameters [2] may be defined to combine the reference temperature evolution with the temperature evolution of any other zone on the surface. For instance a widely used parameter, called "normalized contrast", is defined as:

Table I. Depths and dimensions of defects with reference to the scheme of Figure 2.

	A	B	C
1	depth = 0.25 mm size = 12 x 12 mm	depth = 1.25 mm size = 12 x 12 mm	depth = 2.5 mm size = 12 x 12 mm
2	depth = 0.25 mm size = 6 x 6 mm	depth = 1.25 mm size = 6 x 6 mm	depth = 2.5 mm size = 6 x 6 mm
3	depth = 0.25 mm size = 4 x 4 mm	depth = 1.25 mm size = 4 x 4 mm	depth = 2.5 mm size = 4 x 4 mm

$$C_{i,j}^{n}(\tau) = \frac{T_{i,j}(\tau)}{T_{i,j}^{\max}} - \frac{T_{ref}(\tau)}{T_{ref}^{\max}} \tag{1}$$

where τ is time, $T_{i,j}(\tau)$ and $T_{ref}(\tau)$ are the temperature evolution of the pixel (i, j) and the reference area and T^{max} is the temperature value at the end of heating.

A defect will produce a contrast curve with a maximum value which occurs at a time depending on the depth. Calibration functions, obtained trough numerical simulation or recovered analytically, allow to relate the time of maximum to the defect depth.

Figure 3 shows two images selected from the experimental sequence. A few defects are visible in the first image taken at the beginning of heating; other defects appear in the second one which relates to the very beginning of the cooling stage. Generally, the operator scans the whole sequence trying to find a suitable reference zone and then he proceeds with the thermal tomography algorithm.

In Figure 4 three tomograms are shown. They refer to different layers of material. Defects A1 and A2 are visible in the first one, B1 and B2 in the second one and C1 and C2 in the third one. The fourth image is calibrated in depth units and each gray level represents the defect depth.

From Figure 4, it is clear that noise and artefacts due to uneven heating and 2D diffusion require experience to be distinguished from real defects.

NEURAL NETWORKS

The capability of a Neural Network (NN) to learn basing on experimental data is helpful in solving problems caused by uneven heating and 2D diffusion. In fact, all the parameters involved in the experiment (properties of sound material, defect effects, hardware performance, etc.) contribute to design the NN during the training phase. This allows to develop the heat transfer model which could be hardly achieved using analytical or even numerical methods.

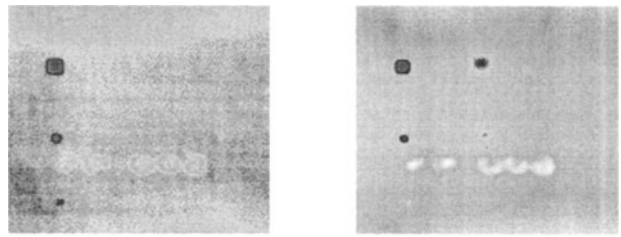

Figure 3. IR images selected from the experimental sequence. Different defects appear at different times. Temperature range is reported.

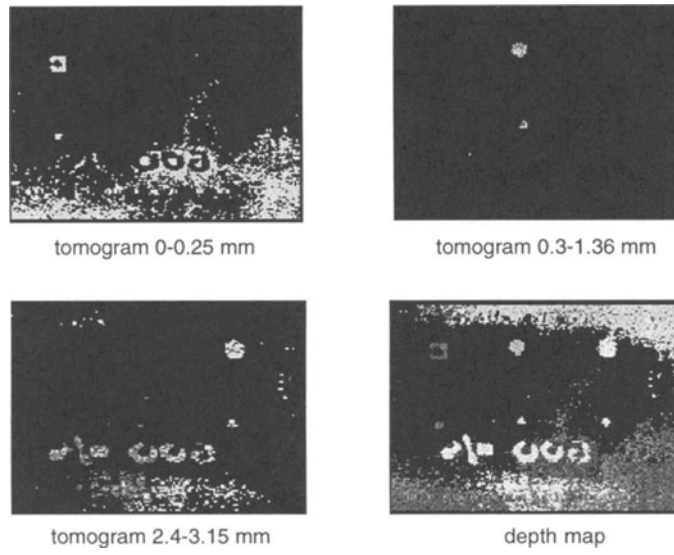

Figure 4. Tomograms obtained from the raw IR sequence by using Thermal Tomography procedure. Different layers present defects at different depths. A defect depth map of the whole specimen is presented too.

Neural Network scheme

We developed two Neural Networks: one for the detection of defects and the other for the characterisation. The second NN operates only on pixels of defects detected by the first one.

The input of the network is a contrast profile in time. A first attempt of training the network with pure temperature profiles did not give satisfying results. The reference value T_{ref} necessary to compute the normalized contrast, is simply the average temperature of the whole sample surface. This avoids the need of an operator to select a suitable non-defect area.

The topology of the network is the result of previous experiences, made on plastic materials [3] [4], and some new improvements. We used feed forward NNs where each layer of neurons (the basic block of a Neural Network) feeds the following one. A NN maps a certain set of input in a set of output, creating a transfer function that is tuned during the training phase. Each elementary block, or neuron, consists of a non-linear sigmoid function. The output of one layer is summed with suitable weights and passed through the sigmoid function. During the training phase the weights are adjusted in order to minimize the global square error between the NN output and the desired one. Because the error is propagated from the output layer back to the previous one, the method of minimization of the error is called Back Propagation.

Figure 5 shows the scheme of the NN used in the defect detection phase. In this specific case the first layer, composed of 37 input neurons, is fed with a contrast profile. The so called hidden layer is composed of 30 neurons and the output layer consists of 20 units for the first NN (detection phase) and 1 unit for the second one (characterisation phase).

Output Layer Structure

There are several possibilities to define the output structure of a NN. To solve identification problems we may have one output neuron with a continuous value from 0 to 1, where 0 means "non-defect" and 1 means "defect"; or we may have two neurons with values from 0 to 1. The first neuron represents the "non-defect" class and the second one the "defect" class. The value of each neuron represents the probability of one pixel to be "defect" or "non-defect". In critical cases, as in the detection phase where a defect and a sound area could have

a similar behaviour, we found that it is better to have many output classes and distribute the expected output as a gaussian function. The optimal standard deviation may be chosen basing on the NN response during the training phase. This solution is more suitable in the presence of noise and when classes of examples are partially overlapped. See Table II.

For the detection NN we used a 20 neuron output layer and we centered the gaussian function on the 7th neuron for the "non-defect" class and on the 13th neuron for the "defect" class. The optimum standard deviation to distribute statistically the output was found to be around three classes. In the recall phase (i.e. using the trained network for the real experiment), the value accepted as output was the center of mass (weighted mean) of all the 20 classes.

Training Set for the Detecting Neural Network

From a sequence of 80 images, originally grabbed during the experiment, many contrast profiles were extracted. Two sets of examples corresponding to the profiles in defect (Figure 6a) and non-defect (Figure 6b) zones were sampled producing the training set for the NN. The examples were selected from different experimental sequences where the position of the sample in the camera field of view was changed. This to take into account the uneven heating distribution. Several pixels corresponding to the writing on the sample surface were used as well. This to introduce examples of signals due to different absorption coefficients in the non-defect training set. In a such a way the NN learns to interpret absorptivity variations as non-defect.

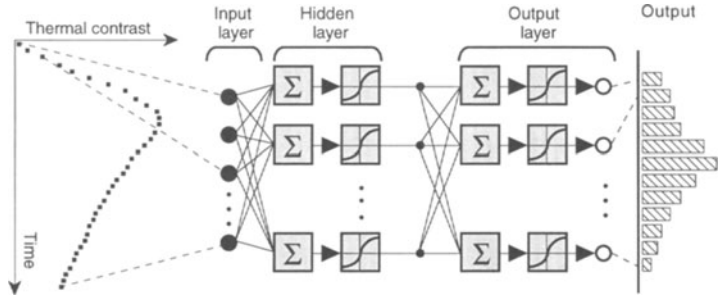

Figure 5. Structure of the neural network used to detect defects. Each input neuron is fed with one value of the thermal contrast profile. Each output represents the probability of a certain class.

Table II. Output structures for the detection NN.

	1 neuron with continuous values from 0 (non-defect) to 1 (defect).
	2 neurons with continuous values from 0 to 1. Class is given by the index of the neuron with the maximum value.
	N neurons with continuous values from 0 to 1. Each class is identified by a gaussian distribution with a given standard deviation (training phase). Class estimation (recall phase) is given by - the index of the neuron with the maximum value; - the center of mass of the output distribution.

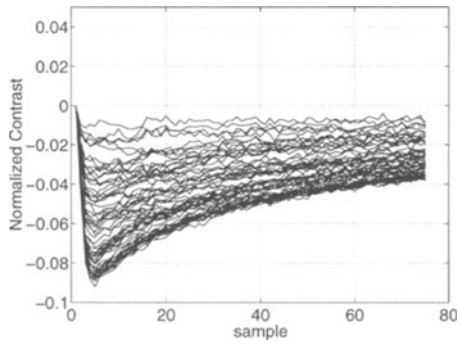

Figure 6a. Training set containing 64 contrast profiles relative to defects A1, A2 e A3.

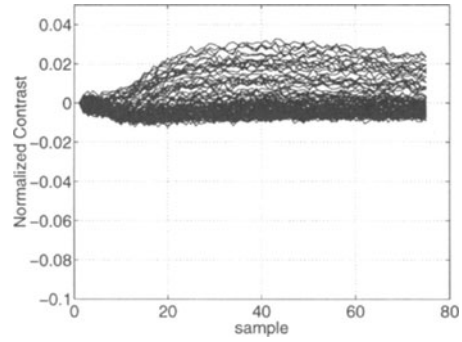

Figure 6b. 100 contrast profiles relative to non-defect areas; the whole training set is composed of 2774 profiles.

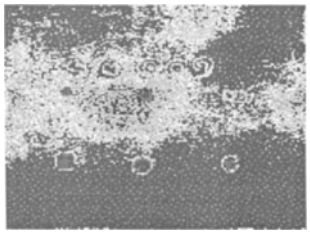

Figure 7a. Output produced by the detecting NN. Output level 1-20.

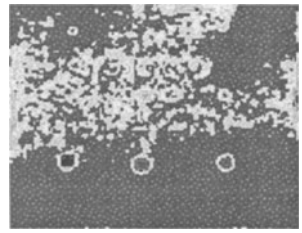

Figure 7b. Image result after the application of a morphological filter (top hat transform).

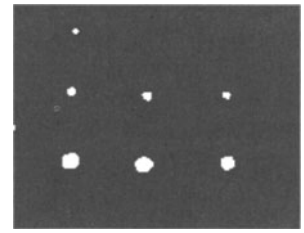

Figure 7c. Binarization of the previous image after thresholding. 7 detected defects.

Output of the Detecting Neural Network

Figure 7a was obtained applying the detecting NN to all the contrast profiles related to the whole sample surface and rearranging the results as an image. Since the network response is the weighted mean of all the 20 output values, Figure 7a appears as an image with gray levels potentially ranging from 1 to 20. Although defects are locally well distinguishable from the surrounding background, some defects and non-defect areas have the same gray level. In such a condition it is not possible to use a global threshold to split the output in two classes of "defect" and "non-defect". The use of a morphological filter (top hat transform) [5], with an opportunely sized mask, makes it possible to separate the background histogram from the defect one (Figure 7b). The choice of the filter mask size is based on the maximum size of defect being looked for. Afterwards, the visibility and location of defects can be enhanced by a simple thresholding (Figure 7c).

Input Data for the Characterising Neural Network

After the detection phase a binary image that represents a map of defect locations is available. For each defect a region of interest is considered (see Figure 8). It is used as a mask to compute the contrast on the original sequence of images. Being the T_{ref} zone selected very close to the defect, effects of uneven heating become negligible. Moreover the processing time is reduced since the NN works only in this more or less small region.

Figure 9 shows some examples obtained with the procedure described above. These contrast profiles represent the new training set for the second (characterizing) NN.

Concerning the output we may say that this phase is less critical than the previous one. Classes of examples coming from defects of different depths are well separated. In this case using the NN as a statistical estimator with multiple output is no more necessary. One output neuron is sufficient indeed. Its level is a real value within the interval [0, 3], even though only the figures 1,2 and 3 represent the depth classes relative to 0.25 mm, 1.25 mm and 2.5 mm respectively. Non-defect points belonging to the region of interest are associated to the 0 value.

Output of the Characterising Neural Network

Figure 10 shows the results of the characterising phase after rounding the real output value to its nearest integer. The NN characterises correctly the defects A1, A2 and A3 in class 1 corresponding to 0.25 mm. Notice some spikes, more critical in the smallest defect, indicating how strong the 2D diffusion effect is for shallow defects. Defects B1 and B2 are also well characterized in class 2 (at a depth of 1.25 mm). Defect B3 contains so few examples, due to its small size and deeper location, that it was not possible to train the net for its recognition. Defect C1 is also recognized in class 3 corresponding to a depth of 2.5 mm. The other two defects were not detected in the first phase.

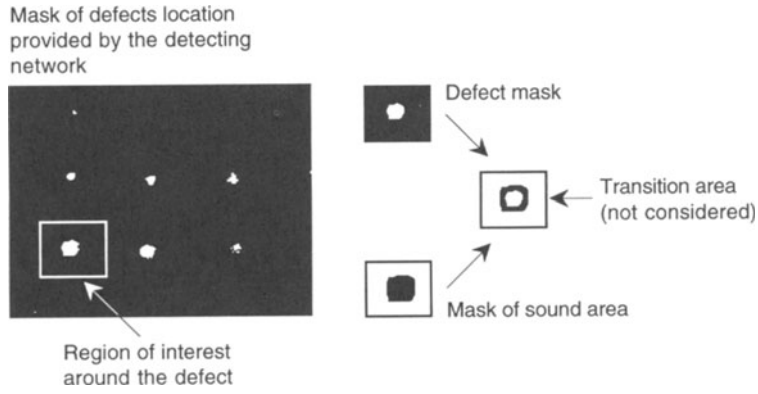

Figure 8. Characterization phase: data extraction.

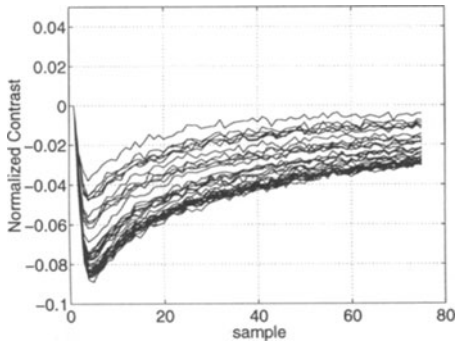

Figure 9a. A1 defect (36 profiles).

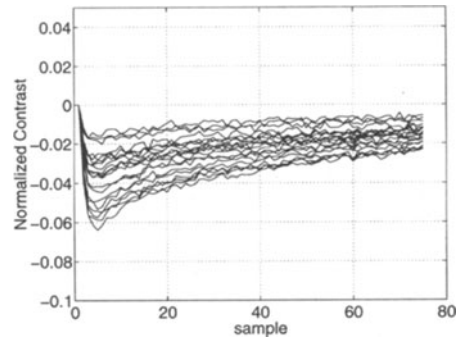

Figure 9b. A2 defect (20 profiles).

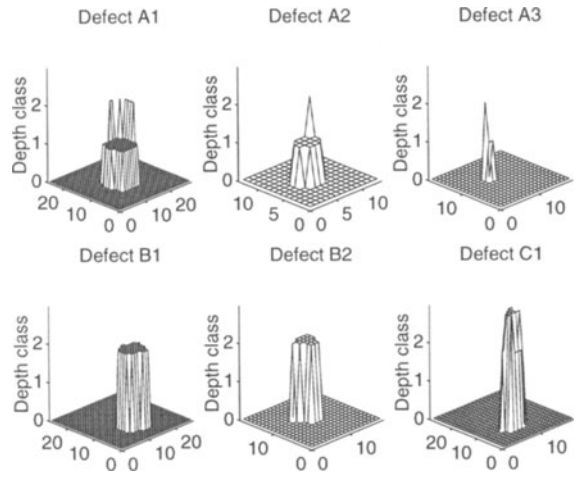

Figure 10. Output of the characterization phase.

CONCLUSION

In conclusion we may state that the NN could learn to identify and characterize defects in CFRP. The results are comparable to those obtained by an expert operator working with some Thermal NDE procedures.

Future works will consist in optimizing the NN to reduce the number of neurons. This will speed up the computation. Other works, more theoretical, regard a deeper understanding of the NN output structure concerning its capability to be a statistical (bayesan) estimator. In field utilization of NN is being developed.

ACKNOWLEDGEMENTS

We wish to thank the Italian Air Force in the persons of R. Capriotti and P. Angelocore for providing us with the CFRP specimen used for this work.

REFERENCES

1. V. Vavilov, P.G. Bison, C. Bressan, E. Grinzato, S. Marinetti, in *QIRT 92 (Quantitative infrared thermography)*, Eurotherm Seminar n. 27, eds. D. Balageas, G. Busse, G.M. Carlomagno, (Editions Europeennes Termique et Industrie, 1992), pp. 259-265.
2. V. Vavilov, P.G. Bison, C. Bressan, E. Grinzato and S. Marinetti, in *Advances in signal processing for non destructive evaluation of materials*, NATO ASI, Series E: Applied Sciences, Vol.262, ed. by X. Maldague (Kluwer Academic Publishers, 1994), pp. 193-207.
3. E. Grinzato, S. Marinetti, P.G. Bison, G. Manduchi, Revue Générale de Termique, tome XXXIV, n. 397, janvier 1995, p. 17-27.
4. P.G. Bison, C. Bressan, R. Di Sarno, E. Grinzato, S. Marinetti, G. Manduchi, in *QIRT 94 (Quantitative infrared thermography)*, Eurotherm Seminar n. 42, eds. D. Balageas, G. Busse, G.M. Carlomagno, (Editions Europeennes Termique et Industrie, 1994), pp. 214-219.
5. P. Zamperoni, *Metodi dell'elaborazione digitale di immagini*, (Masson, Milano, 1990), Chap. 7.